Int. J. Solids Structures Vol. 21, No. 11, pp. 1073–1100, 1985
Printed in Great Britain.

0020-7683/85 $3.00+.00

INELASTIC ANALYSIS OF THIN-WALLED TUBES UNDER CYCLIC BENDING

P. K. SHAW and S. KYRIAKIDES
Engineering Mechanics Research Laboratory, Department of Aerospace Engineering and Engineering Mechanics, University of Texas, Austin, TX 78712, U.S.A.

(*Received* 26 *November* 1984)

Abstract—Thin-walled circular tubes under bending have been shown to ovalize. For tubes bent into the plastic range, part of the ovalization is permanent. It has been demonstrated experimentally that reverse bending and subsequent repeated cyclic bending cause a gradual growth of ovalization. This paper presents a virtual work-type of formulation of the problem in an attempt to analytically predict the growth of ovalization for tubes cycled in pure bending. A number of nonlinear-hardening plasticity models are used in the formulation. The problem solution is found to be sensitive to the choice of hardening rule used.

INTRODUCTION

In many practical applications such as offshore structures, breeder reactor components, earthquake resistant structures, etc., tubular thin-walled structures may be subjected to extreme loads that cause plastic deformations. Earthquake induced motions, wave action and other hostile ambient conditions can cause extended and repeated excursions into the plastic range. Recent experimental and numerical studies have addressed the problems of predicting the response and collapse of tubular (and other) beams, beam columns and frames under inelastic cyclic loading[1–7]. The present study is a detailed examination of the behavior of a tubular element under cyclic inelastic bending.

It is well known that the response of long circular tubes in pure bending is characterized by a limit load. Brazier[8] was the first to relate this nonlinear behavior to the ovalization of the tube cross-section which results from bending. His results were later confirmed by Reissner and Weinitschke[9, 10] in a more complete formulation of the problem. Ades[11] examined the same problem for inelastic material behavior by using the simplifying assumption that the cross-section ovalizes into an elliptical shape. More recently Gellin[12] presented a more complete solution of the elastoplastic problem. These analyses clearly indicated that inelastic tubes possess a moment curvature response which is also characterized by a limit moment. The value of the limit moment, however, is substantially smaller than the one predicted for the linearly elastic material. The Gellin solution was confirmed experimentally and extended to the problem of combined bending and pressure by Kyriakides and Shaw[13]. In view of the "nearly" proportional nature of the stress field, the deformation theory of plasticity was used in [11, 12, 13] with good results. In addition, the tube mid-surface was assumed to be inextensional in the circumferential direction.

One of the important results of [13] was the observation that on unloading a tube bent into the plastic range, a residual permanent ovalization of the cross-section could be measured. This led to the question of what would be the consequences if this initially ovalized tube was reverse bent.† In response to these questions, a cyclic four-point bending facility was developed. Details of the facility and the experimental results are briefly described in [14] and in much more detail in the second paper of this series[15].

Briefly described, the experimental investigations of [15] consist of cyclically loading a tube in pure bending. At a first stage, strictly curvature-symmetric cycles were examined. If we define κ_m as the limit curvature of the monotonic moment–curvature response, then the cyclic experiments were carried out at curvatures of $\kappa_c = \pm\alpha\kappa_m$ where $0 < \alpha < 1$.

---

†This question first arose in discussions between Kyriakides and C. D. Babcock at the California Institute of Technology in 1980.

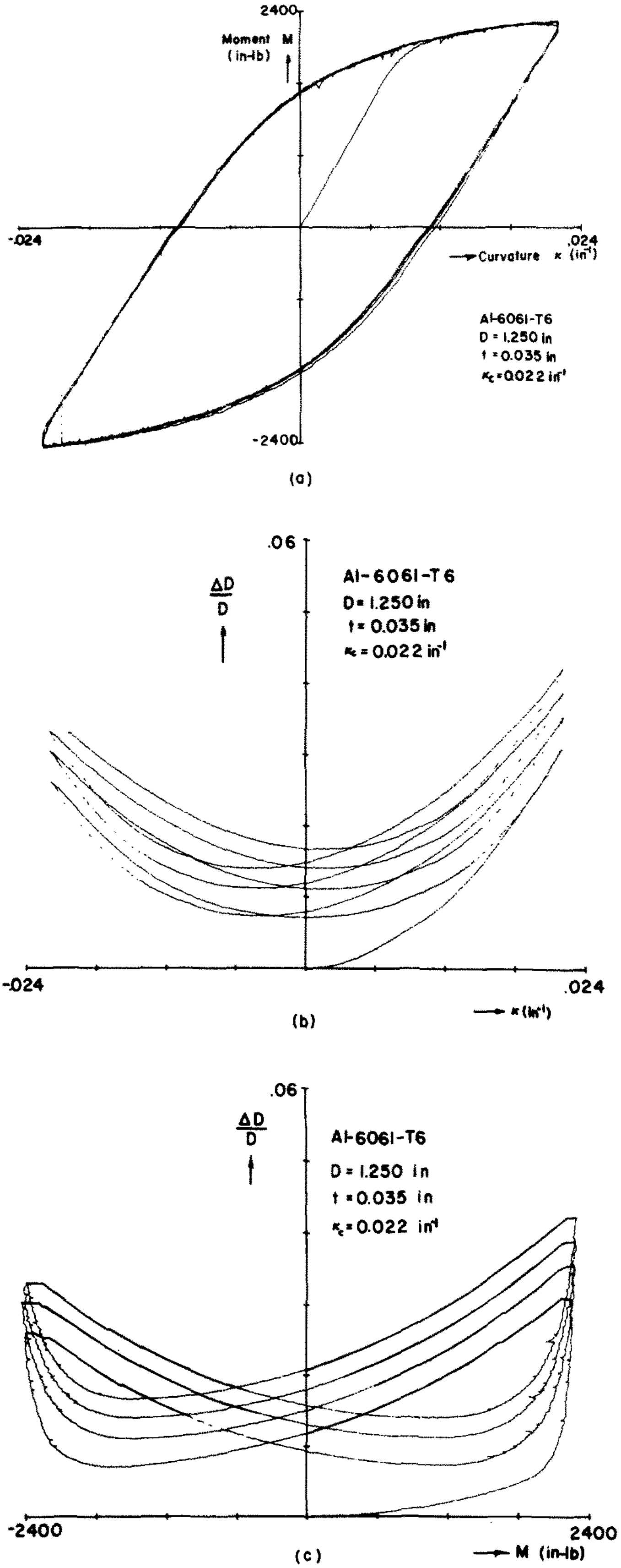

(a)

(b)

(c)

Fig. 1. Cyclic bending response of aluminum tube.

A set of experimentally obtained results is shown in Figs. 1(a)–1(c). Figure 1(a) shows a typical moment–curvature response clearly indicating the hysteretic nature of the inelastic cyclic loading applied. The particular tube tested was 36 in. (.91 m) long, 1.250 in. (31.7 mm) in diameter (O.D.) and 0.035 in. (0.89 mm) thick. The material was aluminum 6061-T6. The cycling curvature (κ_c) was 0.022 in.$^{-1}$ (0.87×10^{-3} mm^{-1}) which is approximately 14% less than the curvature corresponding to the monotonic limit load ($\kappa_m = 0.026$ in.$^{-1}$ and $\alpha = 0.846$). Figure 1(b) shows the change of the minor axis of the tube as a function of the curvature. Figure 1(c) shows the same change in diameter plotted as a function of the applied moment.

It is clear from these results that under cyclic bending the tube "structurally" degrades due to the gradual growth of ovalization. In fact the growth of ovalization can lead to buckling after a number of cycles. The tube shown in Fig. 1 buckled after $3\frac{1}{2}$ cycles. More on the cyclic dependent nature of buckling can be found in [15]. Results from 1018 cold-drawn steel and 304 stainless-steel tubes showed a similar behavior.

This paper presents a formulation and numerical solution of the problem of a long tube cycled in pure bending into the plastic range. The objective is to predict the moment–curvature response and ovalization growth of such a tube. The kinematic formulation is general enough to cover large deflections and circumferential stretching. Due to the bending-induced ovalization the problem requires two-dimensional constitutive relations. For the loading history described, the stressed are nonproportional in nature; as a result, an incremental flow rule is used. In addition, the cyclic nature of the loading dictates proper modeling of cyclic hardening (or softening), creep, relaxation, etc. In view of these complicating factors, a large part of the paper is devoted to the development of the constitutive equations used. A number of different plasticity models have been implemented with particular emphasis on models with nonlinear hardening rules. The predicted structural response is compared to experimental results in an effort to assess the strengths and weaknesses of the constitutive models.

FORMULATION OF THE PROBLEM

(a) *Kinematics*

The problem considered consists of a long thin-walled circular tube of mean radius R and thickness t. The tube is in a state of pure bending, as shown in Fig. 2, which causes a uniform curvature κ. The displacements of a point on the tube's mid-surface, with respect to the axial, circumferential and radial coordinates x, θ and z are u, v and w, respectively.

The kinematic relations required must be general enough to accommodate ovalization of the cross-section. Such a set of relations has been developed in [12] and used successfully in [13]. Briefly, it is assumed that plane sections perpendicular to the tube mid-surfaces before deformation remain plane during deformation. The same assumption is made for bending deformations about the mid-surface of the cross-section. The strains are assumed to remain small but finite rotations about both axes of bending are allowed. The circumferential strain can be expressed as

$$\epsilon_\theta = \epsilon_\theta^0 + z\kappa_\theta, \tag{1}$$

where

$$\epsilon_\theta^0 = \left(\frac{v' + w}{R}\right) + \frac{1}{2}\left(\frac{v' + w}{R}\right)^2 + \frac{1}{2}\left(\frac{v - w'}{R}\right)^2 \tag{2}$$

and

$$\kappa_\theta = \left(\frac{v' - w''}{R^2}\right)\bigg/\sqrt{1 - \left(\frac{v - w'}{R}\right)^2}.$$

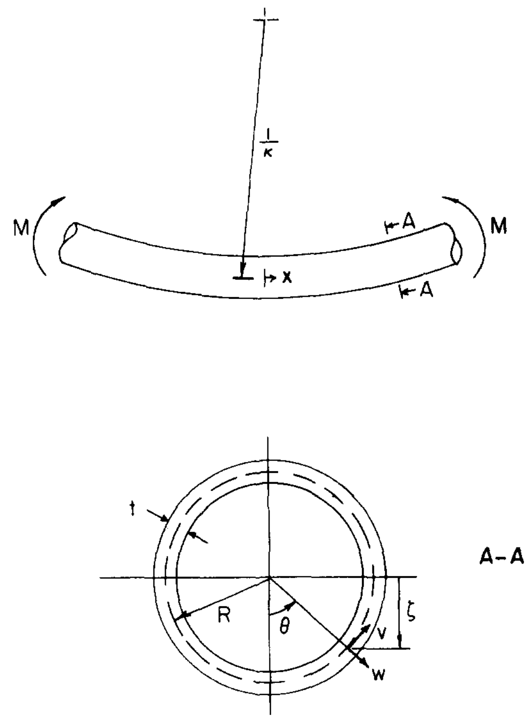

Fig. 2. Problem geometry.

The strain in the direction of the tube axis is given by

$$\epsilon_x = \epsilon_x^0 + \zeta\kappa. \tag{3}$$

From Fig. 2

$$\zeta = [(R + w)\cos\theta - v\sin\theta + z\cos\theta]. \tag{4}$$

Cyclic elastoplastic bending will in general cause shift of the neutral axis as a result ϵ_x^0 generally is not zero.

In order to keep the present formulation as general as possible, the simplifying assumption of inextensionality of the tube's mid-surface in the circumferential direction made in [12] and [13] is relaxed. This will have the effect of doubling the number of nonlinear equations that need to be solved for each load increment.

(b) *Constitutive behavior*

We are interested in examining the behavior of circular tubes under cyclic bending loads with extensive excursions into the plastic range. The induced stress history is highly nonproportional, and as a result the problem must be formulated in terms of incremental plasticity. The formulation used makes use of the simplifying assumptions of the J_2-type of incremental plasticity. Within this theory a number of different hardening rules and two flow rules will be incorporated.

Proper modeling of inelastic cyclic behavior must include cyclic hardening or softening, cyclic creep and cyclic relaxation. The various plasticity models used are presented first assuming the material to be cyclically stable. Cyclic hardening and softening will be incorporated at a second stage.

All models considered belong to the so-called classical plasticity theory. The yield surface, as well as all other surfaces mentioned later, are assumed to be convex. The strain tensor increment is also assumed to allow decomposition into a purely elastic part and a purely plastic part, i.e.

$$\mathrm{d}\epsilon_{ij} = \mathrm{d}\epsilon_{ij}^{e} + \mathrm{d}\epsilon_{ij}^{p}. \tag{5}$$

The normality of $\mathrm{d}\boldsymbol{\epsilon}^p$ to the yield surface is also accepted. Let the yield surface be defined by

$$f(\sigma_{ij} - \alpha_{ij}) = k_0 \tag{6}$$

where k_0 is a material constant and $\boldsymbol{\alpha}$ represents the position of the center of the surface in stress space. Specializing (6) to the J_2-theory

$$f = \tfrac{1}{2}(s_{ij} - a_{ij})(s_{ij} - a_{ij}) = \tfrac{1}{3}\sigma_0^2 \tag{7}$$

where $\mathbf{s}$ is the deviatoric stress tensor, σ_0 is the yield stress obtained from a uniaxial experiment and $\mathbf{a}$ is the center of the surface in the deviatoric stress space.

Two main categories of flow rules are adopted. The first is essentially the one suggested by Drucker and Palgen[16], specifically for use in cases of cyclic loading. The second is the rule on which the Mroz model[17–20] is based. This model incorporates a family of nested surfaces obtained by approximating the uniaxial stress–strain behavior by a series of linear segments.

Following [16] the plastic strain increment can be expressed as

$$\mathrm{d}\epsilon_{ij}^{p} = \frac{1}{H}\frac{(\partial f/\partial\sigma_{mn})\,\mathrm{d}\sigma_{mn}}{(\partial f/\partial\sigma_{pq})(\partial f/\partial\sigma_{pq})}\frac{\partial f}{\partial\sigma_{ij}}. \tag{8a}$$

By adopting (7)

$$\mathrm{d}\epsilon_{ij}^{p} = \frac{1}{H}\frac{(s_{mn} - a_{mn})\,\mathrm{d}s_{mn}}{\tfrac{2}{3}\sigma_0^2}(s_{ij} - a_{ij}). \tag{8b}$$

In the case of a simple uniaxial test (8b) reduces to

$$H = \frac{2}{3}\frac{\mathrm{d}\sigma}{\mathrm{d}\epsilon^p}. \tag{9}$$

Nonlinear hardening stress–strain relationships typical of polycrystalline metal alloys can be approximated through a three-parameter fit (Ramberg–Osgood) as follows:

$$\epsilon^p = \frac{3}{7}\frac{\sigma}{E}\left(\frac{\sigma}{\sigma_y}\right)^{n-1} \tag{10}$$

where E, σ_y and n are material constants. Evaluating H from (10) and adopting the following scalar function definition

$$\sigma_e^2 = \tfrac{3}{2}s_{ij}s_{ij}, \tag{11}$$

(8) can be written as

$$\mathrm{d}\epsilon_{ij}^{p} = \frac{1}{\dfrac{28}{27}\dfrac{E}{n}\sigma_0^2}\left(\frac{\sigma_e}{\sigma_y}\right)^{n-1}[(s_{mn} - a_{mn})\,\mathrm{d}s_{mn}](s_{ij} - a_{ij}). \tag{12}$$

For a hardening or softening material σ_y, E and n depend on the history. This dependence is discussed later. For a cyclically stable material the remaining outstanding problem is that of specifying the way the yield surface moves in stress space.

Hardening rules. For problems with repeated unloading and reverse loading, such as the one considered here, reasonable representation of the Bauschinger effect is essential. Isotropic hardening is obviously unsuitable for such loading. Kinematic hardening was first introduced by Prager[21, 22] and was later modified by Shield and Ziegler[23, 24]. The yield surface is assumed to retain its size and shape and to translate in space. The original Prager hardening rule requires the yield surface to move in the direction of the plastic strain increment, i.e.

$$\mathrm{d}\alpha_{ij} = c\ \mathrm{d}\epsilon_{ij}^{p} \tag{13}$$

where c can be found from the consistency condition. For the Mises-type surface, eqn (7), this can be expressed as

$$(s_{ij} + \mathrm{d}s_{ij} - a_{ij} - \mathrm{d}a_{ij})(s_{ij} + \mathrm{d}s_{ij} - a_{ij} - \mathrm{d}a_{ij}) = \tfrac{2}{3}\sigma_0^2. \tag{14}$$

For some two-dimensional specializations of the theory use of this hardening rule may lead to problems[23]. The Shield–Ziegler hardening rule was suggested as a modification. In this rule the yield surface translates in a direction defined by the line joining the current center of the surface to the stress point. Thus

$$\mathrm{d}\alpha_{ij} = \mathrm{d}\mu(\sigma_{ij} - \alpha_{ij}); \tag{15}$$

$\mathrm{d}\mu$ can be evaluated from the consistency condition (14).

Extended Phillips hardening rule. Phillips and Lee in [25], summarized a number of experimentally based observations regarding the existence and kinematics of yield and loading surfaces. They reemphasized the notion of a "super" surface which represents the largest state of stress achieved in the loading history. This surface, given the name "loading surface," encloses the yield surface at all times. According to [25] the loading surface expands isotropically each time the loading prescribes higher stress. The yield surface encloses strictly the "elastic region"[26]. The yield surface was observed to move "predominantly" in the direction of the stress increment if it occupies a position "far" enough from the loading surface. This phenomenon was also observed by Michno and Findley[27] based on independent experiments. [26] also states that the yield surface "tends to become tangential to the loading surface if close to it." Since movement of the yield surface along $\mathrm{d}\boldsymbol{\sigma}$ will, in general, cause the two surfaces to intersect, the last observation implies that a "loading-surface–influenced region" exists. In this region the yield surface moves in such a way so as to ensure that the two surfaces become tangent to each other whenever they come into contact. Unfortunately, the size of the regime where the yield surface "senses" the existence of the loading surface beyond has not been quantified to date.

In what follows, a two-surface plasticity model and associated hardening and flow rules are presented. They are tailored to fit most of the above observations. Motivated by the needs of the structural problem at hand, a number of practical innovations are added to the basic ideas put forward in [25]. These will be pointed out for critical review by the reader.

The model makes use of two surfaces. The loading surface can be viewed as a super surface enclosing all activity in the stress space. This surface is taken to be centered at $\boldsymbol{\sigma} = 0$, and is defined by the maximum value a function $f(\sigma_{ij})$ has attained in the loading history, i.e. the surface is given by

$$f(\sigma_{ij})_{\max} = k. \tag{16}$$

Specifying this surface as a Mises surface,

$$f(\sigma_{ij})_{\max} = J_2^{\max} = \tfrac{1}{3}\sigma_m^2, \qquad J_2 = \tfrac{1}{2}s_{ij}s_{ij}. \tag{17}$$

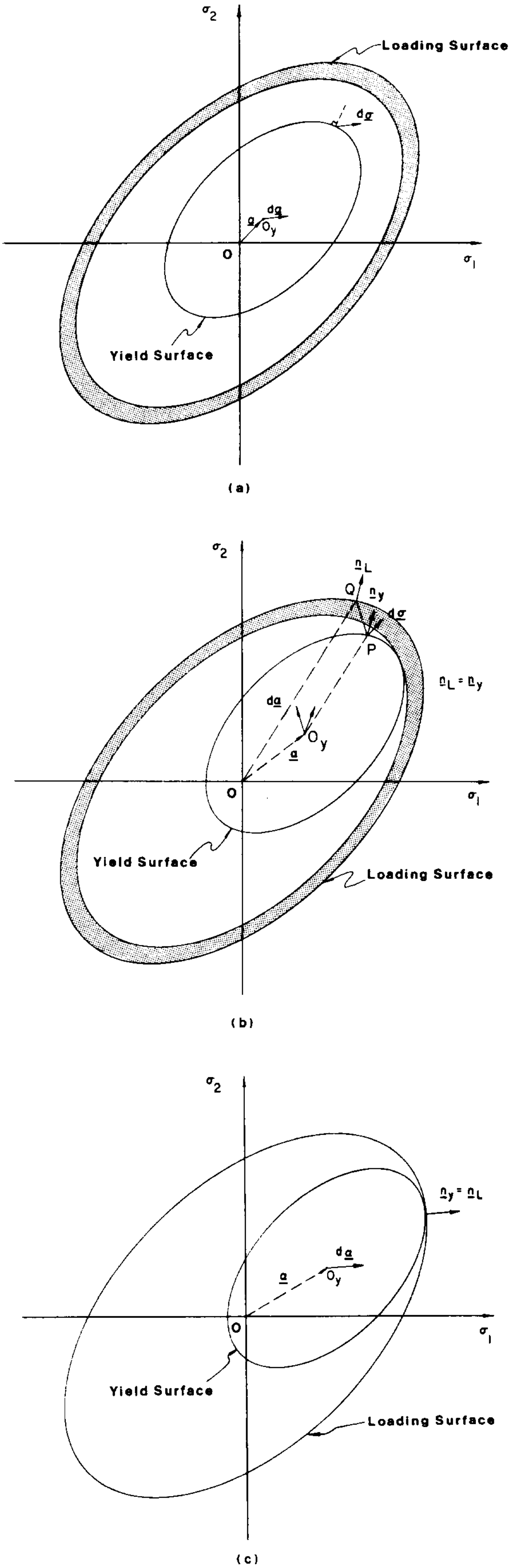

Fig. 3. Extended Philips hardening rule.

When the yield surface comes into contact with the loading surface, any further loading is such as to cause isotropic growth of this surface. The yield surface is again defined by eqns (6) and (7).

The following hardening rule is adopted in order to satisfy the *spirit* of the experimental observations in [25] regarding the motion of subsequent yield surfaces:

$$da_{ij} = d\mu\{[1 - h(\xi)]n_{ij}^{(1)} + h(\xi)n_{ij}^{(2)}\}, \tag{18}$$

where $\mathbf{n}^{(1)}$ is the unit vector in the stress-increment direction, and $\mathbf{n}^{(2)}$ is the unit vector in the direction that the yield surface should follow to ensure tangency with the loading surface on intersection. ξ is a measure of the normalized distance between the two surfaces and is taken as

$$\xi = \frac{1}{\sigma_0}[\sigma_m - \sqrt{3J_2(a_{ij} + ds_{ij})} - \sigma_0]. \tag{19}$$

$h(\xi)$ is an unknown function of ξ which governs the mixed hardening rule represented by eqn (18). In view of the limited experimental information available on the subject, the following simple representation is adopted for $h(\xi)$:

$$h(\xi) = \begin{cases} 0, & \xi < \xi_0, \\ 1, & \xi \geqq \xi_0 \end{cases}, \qquad \xi_0 = \frac{\beta}{\sigma_0}(\sigma_m - \sigma_0), \tag{20}$$

where β is a material constant. (20) establishes a band of width $\xi_0\sigma_0$ concentric with the loading surface just inside the loading surface. If the yield surface is in contact or intersects this band then

$$da_{ij} = d\mu n_{ij}^{(2)}; \tag{21}$$

otherwise

$$da_{ij} = |ds|\, n_{ij}^{(1)}, \qquad |ds| = [ds_{ij}\, ds_{ij}]^{1/2}. \tag{22}$$

Figures 3(a), 3(b) and 3(c) show pictorially the implications of (18) and (19). In Fig. 3(a),

$$J_2(a_{ij} + ds_{ij}) < \tfrac{1}{3}[\sigma_m - (\xi_0 + 1)\sigma_0]^2, \tag{23}$$

then

$$da_{ij} = ds_{ij}. \tag{24}$$

In Fig. 3(b), the stress state satisfies

$$J_2(a_{ij} + ds_{ij}) \geqq \tfrac{1}{3}[\sigma_m - (\xi_0 + 1)\sigma_0]^2 \tag{25}$$

and

$$J_2(s_{ij} + ds_{ij}) < \tfrac{1}{3}\sigma_m^2,$$

then from (21),

$$da_{ij} = d\mu(\hat{s}_{ij} - s_{ij})/[(\hat{s}_{kl} - s_{kl})(\hat{s}_{kl} - s_{kl})]^{1/2}. \tag{26}$$

$\hat{\mathbf{s}}$ represents **OQ** in Fig. 3(b), and $\mathbf{n}^{(2)}$ the unit vector along **PQ**. This construction is due to Mroz[18], and represents the direction that must be followed by the yield surface to ensure it becomes tangential to the loading surface. From Fig. 3(b)

$$\hat{s}_{ij} = \frac{\sigma_m}{\sigma_0}(s_{ij} - a_{ij}). \tag{27}$$

$d\mu$ in (26) can be calculated from the consistency condition. If $J_2(s_{ij} + ds_{ij}) > \frac{1}{3}\sigma_m^2$, i.e. for loading beyond the current position of the loading surface, the yield surface remains tangential to the loading surface at the current position of stress. The stress path is thus governed by the isotropic growth of the loading surface. The initial monotonic loading is also governed by isotropic hardening with the yield surface attached to the loading surface at the point of the stress vector.

In summary, the rule presented has three hardening regimes: one for loading beyond the previous maximum stress state, and two for paths inside the surface representing the maximum stress state. The choice between the latter two depends on the proximity of the yield surface to the loading surface described by the parameter β. The adoption of the particular functional description of $h(\xi)$ given by (23) represents an effort by the authors to keep the model as simple as possible. However, even this representation contains a material parameter β which requires experimental determination.

Cyclic hardening. The discussion of constitutive equations above has been restricted to "cyclically stable" materials. It is well known that the response under cyclic loads of most metals is much more complex than presented above. Presented in [28–31] is a wealth of experimental data which illustrate cyclic hardening and softening, cyclic relaxation and cyclic creep, as well as other not easily classified phenomena exhibited by polycrystalline materials under cyclic loads. Figure 4(a) shows results from a uniaxial test on aluminum 6061-T6. The material is clearly seen to harden under strain-symmetric cycling.

Efforts to model time-independent cyclic phenomena have been presented, among others, by Eisenberg[32], Caulk and Naghdi[33] and Drucker and Palgen[16]. Included in [16] is a nonlinear stress–strain relation which in its nonhardening (stable) form, reduced to (12). The model introduces a hardening (or softening) parameter which is a function of the plastic work done (see eqns (22–25) in [16]). Parameters E, σ_y and n [see eqn (10)] are obtained from the upper or lower half of the stable hysteresis loop [Fig. 4(c)]. In addition, cyclic hardening is incorporated by making σ_y in (12) to be history dependent.

The above model constitutes the main tool for establishing the elastoplastic stress state during the cyclic history applied to the structural elements examined in this paper. Although the spirit of [16] is followed diligently, a few changes, most due to personal preference, have been implemented. The most serious deviation from the model, as presented in [16], was introduced by the additional requirement that the stable hysteresis loop coincide with the "cyclic stress–strain curve" for all strain-symmetric cyclic tests. The addition of this requirement was found to yield slightly better agreement between experimental and numerical uniaxial cyclic tests.

For most metals the monotonic loading stress–strain curve is rather different from the stable hysteresis loop. In view of the fact that some of the structural applications we examined were only cycled 1–3 cycles, it was thought prudent to fit this curve separately. Thus, the version of the model used in this program requires input data representing three uniaxial stress–strain curves [see Fig. 4(c)]; the monotonic loading curve (OB), the stable hysteresis loop (PQR) and the cyclic stress–strain curve (OPA). Each was extracted from uniaxial experiments carried out on specimen of the same material as that of the tube used. Each was fitted with a three-parameter fit (Ramberg–Osgood). The definition of the cyclic stress–strain curve is given in [29]. It is customarily obtained through an incremental cyclic stress–strain test. Part of such a test is shown in Fig. 4(b).

Further details on the way these modifications were implemented can be found in Appendix I.

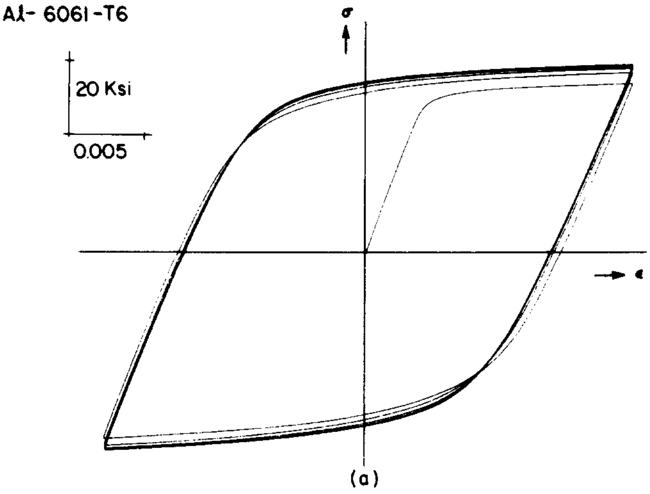

Cyclic Hardening Behavior of Al-6061-T6.

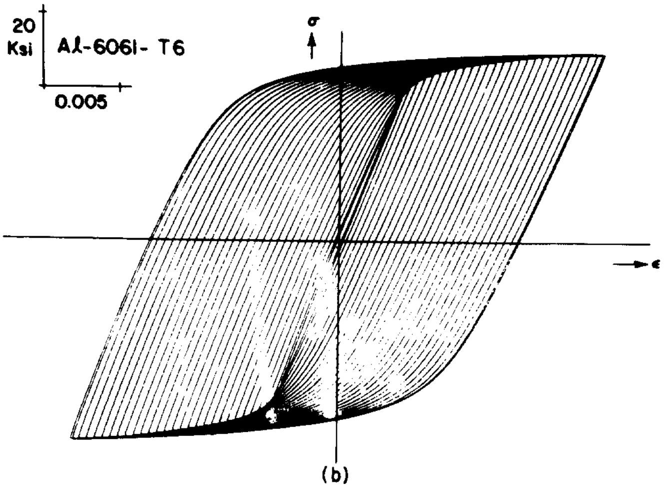

Incremental Cyclic Stress-Strain Test Used to Cyclically Stabilize the Material.

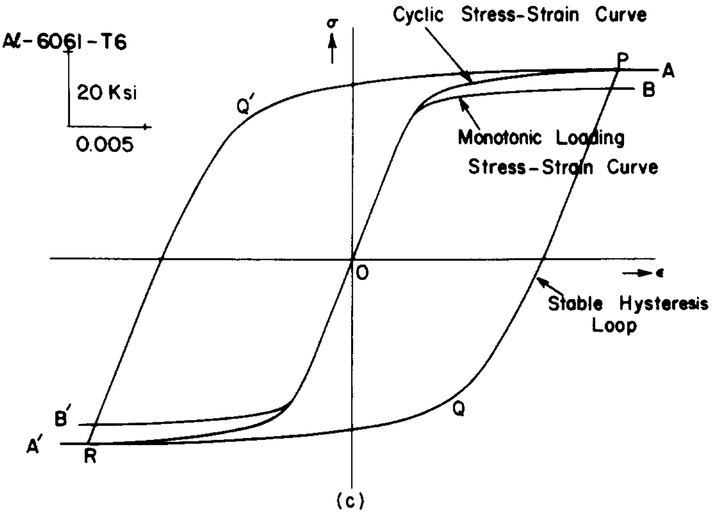

Definition of Stress-Strain Curves Used in Models.

Fig. 4. Uniaxial cyclic stress–strain experimental results.

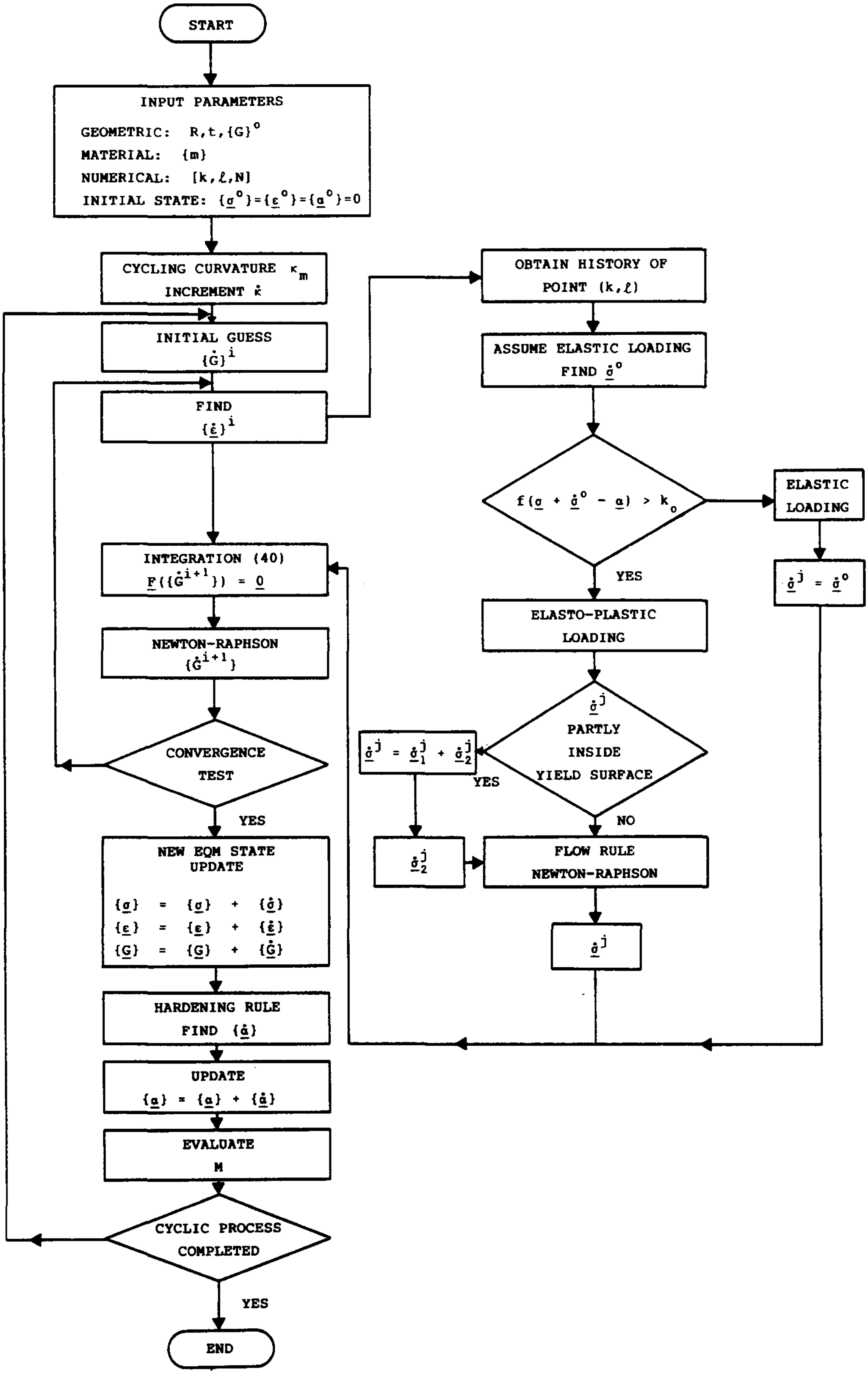

Fig. 5. Flow chart of numerical solution procedure.

(c) *The principle of virtual work*

The requirement of equilibrium is introduced through the principle of virtual work which can be stated as

$$\int_V \sigma_{ij}\delta\epsilon_{ij}\,\mathrm{d}V = \delta W \tag{28}$$

where δW represents the virtual work of the external loads and V the volume of the material of the section of tube considered. For the problem at hand, $\delta W = 0$ since the curvature κ will be prescribed. For incremental loading (28) becomes

$$\int_V (\sigma_{ij} + \dot{\sigma}_{ij})\delta\dot{\epsilon}_{ij}\,\mathrm{d}V = 0 \tag{29}$$

where σ_{ij} represents the stress state in the immediately previous equilibrium state. $(\dot{\cdot})$ indicates rate (for numerical purposes, the increment). For the problem considered, eqn (29) can be reduced to

$$2R\int_0^{\pi}\int_{-t/2}^{t/2}[(\sigma_x + \dot{\sigma}_x)\delta\dot{\epsilon}_x + (\sigma_\theta + \dot{\sigma}_\theta)\delta\dot{\epsilon}_\theta]\,\mathrm{d}z\,\mathrm{d}\theta = 0. \tag{30}$$

From eqns (3) and (4)

$$\begin{aligned}\delta\dot{\epsilon}_x &= \delta\dot{\epsilon}_x^0 + [\delta\dot{w}\cos\theta - \delta\dot{v}\sin\theta]\hat{\kappa},\\ \delta\dot{\epsilon}_\theta &= \delta\dot{\epsilon}_\theta^0 + z\delta\dot{\kappa}_\theta\end{aligned} \tag{31}$$

where

$$\hat{\kappa} = \kappa + \dot{\kappa}. \tag{32}$$

$$\delta\dot{\epsilon}_\theta^0 = \frac{1}{R^2}\{[R + (\hat{v}' + \hat{w})](\delta\dot{v}' + \delta\dot{w}) + (\hat{v} - \hat{w}')(\delta\dot{v} - \delta\dot{w}')\}$$

and

$$\delta\dot{\kappa}_\theta = \frac{1}{R^2}\left\{\frac{(\delta\dot{v}' - \delta\dot{w}'')[1 - (\hat{v} - \hat{w}')^2/R^2] + (\hat{v}' - \hat{w}'')(\hat{v} - \hat{w}')(\delta\dot{v} - \delta\dot{w}')/R^2}{[1 - (\hat{v} - \hat{w}')^2/R^2]^{3/2}}\right\} \tag{33}$$

where $\hat{\mathbf{u}} = \mathbf{u} + \dot{\mathbf{u}}$, $\mathbf{u}$ being the previous equilibrated value of the variable and $\dot{\mathbf{u}}$ the variable rate (or increment). Substituting (31), (32) and (33) into (30)

$$\int_0^{\pi}\int_{-t/2}^{t/2}\{\hat{\sigma}_x\delta\dot{\epsilon}_x^0 + A\delta\dot{v} + B\delta\dot{w} + C\delta\dot{v}' + D\delta\dot{w}' + E\delta\dot{w}''\}\,\mathrm{d}z\,\mathrm{d}\theta = 0$$

where

$$\begin{aligned}A &= -\hat{\sigma}_x\hat{\kappa}\sin\theta + \hat{\sigma}_\theta\left\{\left(\frac{\hat{v} - \hat{w}'}{R^2}\right) + \frac{z}{R^2}\left(\frac{(\hat{v}' - \hat{w}'')(\hat{v} - \hat{w}')/R^2}{[1 - (\hat{v} - \hat{w}')^2/R^2]^{3/2}}\right)\right\},\\ B &= \hat{\sigma}_x\hat{\kappa}\cos\theta + \hat{\sigma}_\theta\left(\frac{R + \hat{v}' + \hat{w}}{R^2}\right),\\ C &= \hat{\sigma}_\theta\left\{\left(\frac{R + \hat{v}' + \hat{w}}{R^2}\right) + \frac{z}{R^2}\left(\frac{1}{[1 - \hat{v} - \hat{w}')^2/R^2]^{1/2}}\right)\right\},\\ D &= \hat{\sigma}_\theta\left\{-\frac{(\hat{v} - \hat{w}')}{R^2} + \frac{z}{R^2}\left(\frac{(\hat{v}' - \hat{w}'')(\hat{v} - \hat{w}')/R^2}{[1 - (\hat{v} - \hat{w}')^2/R^2]^{3/2}}\right)\right\},\\ E &= -\hat{\sigma}_\theta\left\{\frac{z}{R^2}\left(\frac{1}{[1 - (\hat{v} - \hat{w}')^2/R^2]^{1/2}}\right)\right\}.\end{aligned} \tag{34}$$

NUMERICAL SOLUTION

The tube is assumed to deform symmetrically about the $\theta = 0$ line (Fig. 2). The displacements w and v, both functions of θ, are approximated by the following series expansions[12]:

$$w \cong R \sum_{n=0}^{N} a_n \cos n\theta, \qquad v \cong R \sum_{n=2}^{N} b_n \sin n\theta. \tag{35}$$

Substituting (35) into (34)

$$\int_0^{\pi} \int_{-t/2}^{t/2} \left\{ \hat{\sigma}_x \delta\epsilon_x^0 + R \sum_{n=0}^{N} [(B \cos n\theta - Dn \sin n\theta - En^2 \cos n\theta)\, \delta\dot{a}_n] \right. \\ \left. + R \sum_{n=2}^{N} [(A \sin n\theta + Cn \cos n\theta)\, \delta\dot{b}_n] \right\} dz\, d\theta = 0. \tag{36}$$

In view of the arbitrariness of $\delta\dot{\epsilon}_x^0$, $\delta\dot{a}_n$ and $\delta\dot{b}_n$ for all n, the following equations can be extracted from (36):

$$\int_0^{\pi} \int_{-t/2}^{t/2} \hat{\sigma}_x \, dz\, d\theta = 0,$$

$$\int_0^{\pi} \int_{-t/2}^{t/2} (B \cos n\theta - Dn \sin n\theta - En^2 \cos n\theta)\, dz\, d\theta = 0, \qquad n = 0, 1, \ldots, N,$$

$$\int_0^{\pi} \int_{-t/2}^{t/2} (A \sin n\theta + Cn \cos n\theta)\, dz\, d\theta = 0, \qquad n = 2, 3, \ldots, N, \tag{37}$$

where A, B, C, D, E and $\hat{\sigma}_x$ are functions of $\{a_n, b_n, \epsilon_x^0\}$, $\{\dot{a}_n, \dot{b}_n, \dot{\epsilon}_x^0\}$, $n = 0, 1, \ldots, N$, and history. $\{a_n, b_n, \epsilon_x^0\}$ represent the previous solution and are known. Thus at any stage in the incremental solution process, eqns (37) when integrated reduce to $(2N + 1)$ algebraic nonlinear equations in terms of $\{\dot{a}_n, \dot{b}_n, \dot{\epsilon}_x^0\}$, which are solved numerically using the Newton–Raphson method. It is important to note that in the elastoplastic case the procedure has to involve knowledge of the current state of stress and history on which the material properties depend.

The main steps of the numerical solution of (37) are shown in a flow chart in Fig. 5. The half-tube cross-section is represented by k and l Gaussian points in the θ and z directions respectively, in order to facilitate the numerical integration of eqns (37).

The solution procedure is started by prescribing the geometric, material and degree-of-freedom parameters and initializing the stresses. Initial geometric imperfections of the tube cross-section and initial stresses can be prescribed if chosen.

The solution is controlled by prescribing the tube curvature (κ). The first value of κ used is usually small, representing strictly elastic deformations. The closed-form elastic Brazier solution[8] is used to obtain the first initial guess. For subsequent increments of κ, the previous converged solution is used as initial guess. The initial guess involves the displacements. The strain increments are subsequently calculated, and the subroutine dealing with stress–strain relations is called to calcuate the stress increments at every one of the integration points.

Elastic loading is assumed as a first step. The stress increments calculated are added to the previous stress state and the yield criterion is used to establish whether yield has occurred. If yielding has not occurred, then the stress increments are accepted and the procedure continues by returning to the integration of (37). If yielding has occurred, then the full elastoplastic formulation must be used. Using eqn (5), the assumption that for thin-walled tubes the normal stress can be neglected, and by utilizing eqn (12) the following expressions can be written between the relevant strain and stress increments:

$$\begin{aligned} d\epsilon_x &= \frac{d\sigma_x}{E} - \nu\frac{d\sigma_\theta}{E} + \frac{1}{6H\sigma_0^2}(2\hat{\sigma}_x - \hat{\sigma}_\theta)\,[(2\hat{\sigma}_x - \hat{\sigma}_\theta)\,d\hat{\sigma}_x + (2\hat{\sigma}_\theta - \hat{\sigma}_x)\,d\hat{\sigma}_\theta] \\ d\epsilon_\theta &= \frac{d\sigma_\theta}{E} - \nu\frac{d\sigma_x}{E} + \frac{1}{6H\sigma_0^2}(2\hat{\sigma}_\theta - \hat{\sigma}_x)\,[(2\hat{\sigma}_x - \hat{\sigma}_\theta)\,d\hat{\sigma}_x + (2\hat{\sigma}_\theta - \hat{\sigma}_x)\,d\hat{\sigma}_\theta] \end{aligned} \tag{38}$$

where $\hat{\sigma}_x = \sigma_x - \alpha_x$ and $\hat{\sigma}_\theta = \sigma_\theta - \alpha_\theta$. For the case of loading from an already yielded state, these equations are used to calculate the stress increments. The process is an iterative one as it involves updating of the state of stress and the position of the yield surface. If the loading originates from an elastic state but becomes plastic due to the increment of the strain applied, then the following procedure is used. The stress increment $d\boldsymbol{\sigma}$ is expressed as

$$d\boldsymbol{\sigma}_1 = r\,d\boldsymbol{\sigma}, \qquad d\boldsymbol{\sigma}_2 = (1 - r)\,d\boldsymbol{\sigma},$$

where $r\,d\boldsymbol{\sigma}$ is the part of the stress increment which is elastic. r can be evaluated from the yield condition and then the part of the strain increment corresponding to this stress can be separated. Once this is done, the previous procedure is used to calculate the actual stress increment.

Once the stresses at every Gaussian point are evaluated, eqns (37) are integrated numerically. This reduces (37) to $(2N + 1)$ algebraic nonlinear equations which are solved iteratively using the Newton–Raphson method. Convergence is reached as the change in the value of $\{\dot{a}_n, \dot{b}_n, \dot{\epsilon}_x^0\}$ used in the iteration has a norm less than a small quantity specified. At this time the stresses, strains and deflections are updated. In addition, the new position of the yield surface, at every integration point, is updated using one of the hardening rules described in the previous section. Additional information stored in memory are the maximum stress in the history for every point, and parameters needed for calculating the changes induced to the stress–strain curve from cycling. Cyclic loading is achieved by the prescription of the value of κ. Typically, the curvature was varied between $\pm\alpha\kappa_m$.

A number of preliminary exercises were run first in order to check the suitability of the choice of number of expansion terms N in (35), the number of integration points used (k and l), as well as the appropriateness of the strain–displacement relations used in eqn (2). Figures 6(a) and 6(b) show the sensitivity of the bending–curvature and ovalization–curvature responses for monotonic loading to the number of expansion terms used in (35). It is clearly demonstrated that for monotonic loading $N = 4$ or 6 is sufficient. A parametric study demonstrated the choice of $k = 12$ and $l = 5$ to be adequate.

Figures 7(a) and 7(b) show the large deflection bending–curvature and ovalization–curvature response for linearly elastic material. Results from [13] (linear curvature displacement relationship, inextensional circumferential deformations, doubly symmetric deformations assumed); from the current formulation using a linear curvature displacement relationship (extensional circumferential deformations, symmetry only about the axis in the plane of applied moment); from the current formulation using the general strain–displacement relationships as in (2); and results obtained using the general large deformation code ABAQUS[34] (shell formulation). The results are normalized by the critical values

$$M_m^e = \frac{2\sqrt{2}}{9}\,\pi\,\frac{E}{\sqrt{(1 - \nu^2)}}\,Rt^2, \qquad \kappa_m^e = \frac{\sqrt{2}}{3}\,\frac{1}{\sqrt{(1 - \nu^2)}}\left(\frac{t}{R^2}\right), \tag{39}$$

obtained by Brazier[8] in his closed-form small deflection, linearized strain–displacement formulation with circumferentially inextensional mid-surface and doubly symmetric deformation field. It is clear that up to the limit load all formulations predict

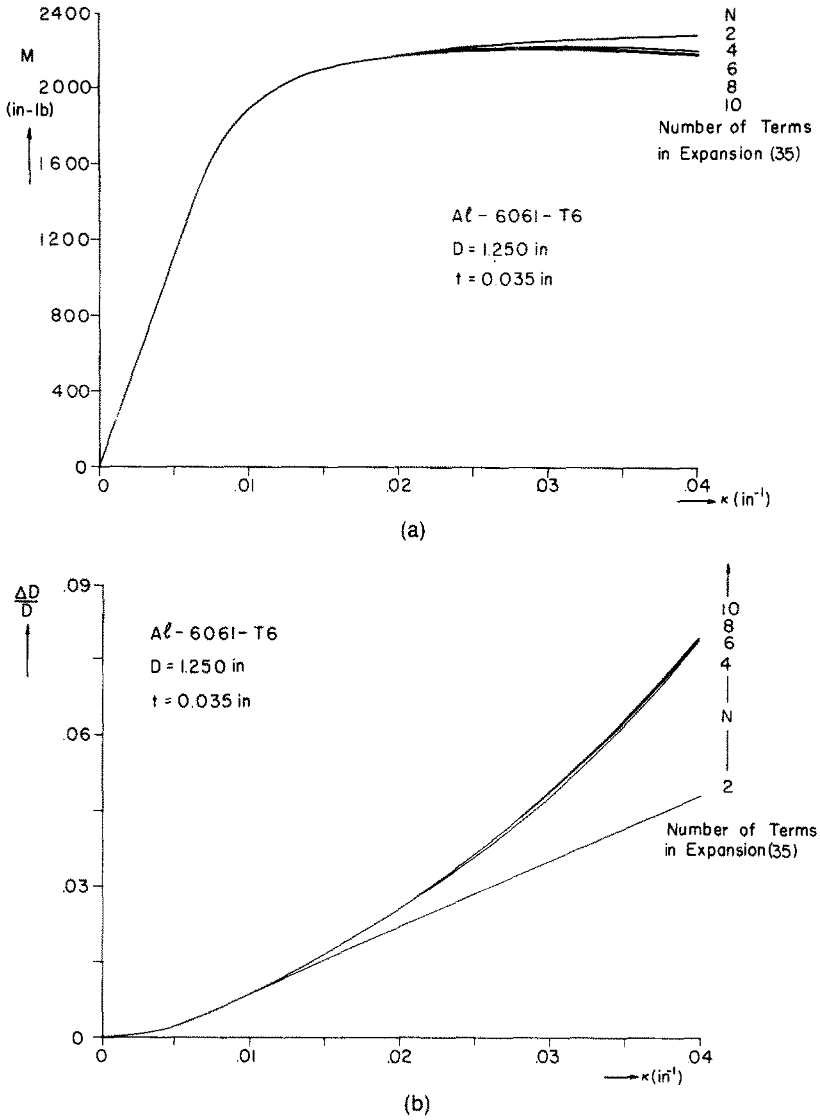

Fig. 6. (a) Predicted monotonic M-κ response for different number of terms in expansion (35). (b) predicted ovalization for monotonic loading for different number of terms in expansion (35).

reasonably close results. The predicted critical curvatures, moments and ovalizations are tabulated below.

	M_m/M_m^e	κ_m/κ_m^e	$\Delta D_m/D$
Nonlinear κ_θ	0.970	1.009	0.256
Linear κ_θ	0.944	0.939	0.234
Doubly symmetric	0.950	0.957	0.241

It must be emphasized that the limit load for the elastic case occurs at values of $\Delta D/D \cong 0.25$, which is a rather tough test for all formulations using linearized strain–displacement relations. The two linearized versions of the formulation are seen to deviate substantially beyond the limit load. However, the complete formulation used in this paper is shown to be in very good agreement with the results predicted by the ABAQUS code. As pointed out by Fabian[35, 36] the deformation of the cross-section is not doubly symmetric. The effect of assuming double symmetry can cause an error for deformations larger than those represented by the critical load for the elastic case.

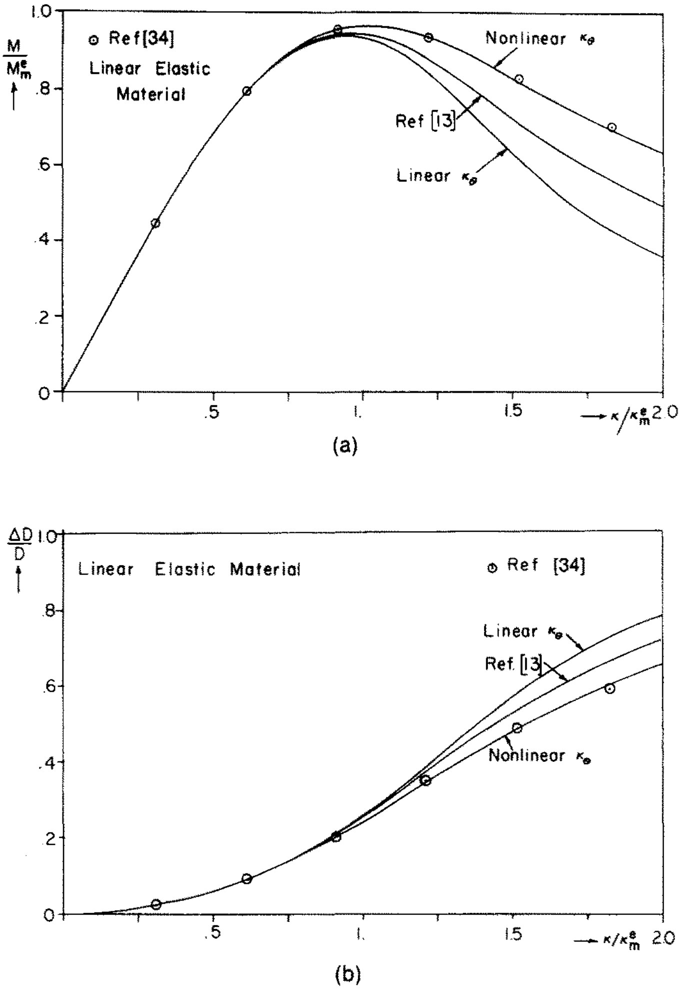

Fig. 7. (a) Large deflection moment curvature response predicted using various kinematic relations. (b) Large deflection ovalization predictions from various kinematic relations (elastic case).

The above test has been carried out in order to add confidence to the kinematic relations used. The reader is reminded that in the elastoplastic case the critical load occurs at deformation levels of the cross-section 4 to 5 times smaller than the values obtained in the elastic case. For this reason neglecting $\dot{\epsilon}_x^0$, assuming the inextensional deformation[12] and using linearized values of κ_θ are acceptable simplifications as demonstrated in [13]. For completeness the kinematic formulation used in this paper is the fully nonlinear one represented by (2). In addition, only one plane of symmetry has been assumed, which results to the presence of $\dot{\epsilon}_x^0$ in the formulation.

RESULTS AND DISCUSSION

We proceed to evaluate the performance of the various plasticity models discussed earlier in attempts to predict the moment–curvature response and ovalization growth of inelastic tubes cycled in pure bending. The discussion will be based on calculations for a long tube, 1.25 in. (31.7 mm) in diameter (O.D.) and 0.035 in. (0.89 mm) thick. Strictly curvature-symmetric cycles are considered. The tube material was aluminum 6061-T6. The material properties of this type of aluminum were obtained from a separate set of uniaxial experiments (Fig. 4). Parameters representing the monotonic stress–strain curve, the cyclic stress–strain curve and the stable hysteresis loop, as defined in Fig. 4(c), are listed in Fig. 8.

	E_l	σ_{yl}	n_l
Monotonic $\sigma-\epsilon$	9.2×10^6 psi (63.4 GPa)	43×10^3 psi (297 MPa)	2.5

	E_s	σ_{ys}	n_s
Stable Hysteresis Loop	9.2×10^6 psi (63.4 GPa)	9.1×10^3 psi (62.7 MPa)	1.5

	E_c	σ_{yc}	n_c
Cyclic $\sigma-\epsilon$	9.2×10^6 psi (63.4 GPa)	42×10^3 psi (290 MPa)	1.0

Yield Surface Radius, σ_0 : 30×10^3 psi (207 MPa)

Hardening Parameter, A : 0.7

$\beta = 0.333$

Fig. 8. Material parameters used.

The predictions for strictly monotonic loading are first compared (see Fig. 9). The limit moments and curvatures predicted by each model are as follows:

	M_c(in. lb.)	κ_c(in.$^{-1}$)
Deformation theory	2204	0.027
Kinematic hardening (Ziegler)	2206	0.0275
Isotropic hardening	2213	0.0292
Kinematic hardening (d_σ direction)	2243	0.0375

When compared to experiment, deformation theory has 3.8% difference in κ_c, kinematic hardening (Ziegler) 5.8%, isotropic hardening 12.3% and kinematic hardening with the yield surface moving in the direction of the stress increment d_σ, differ by 49%. It must be emphasized that the kinematic hardening used here is the one represented by eqns (12) and (13). The results presented for this type of hardening are based on the choice of yield surface radius of $\sigma_0 = 30{,}000$ psi (207 MPa).

Figure 9(b) shows the corresponding ovalization–curvature results. The first three models yield ovalization predictions which are reasonably close up to the limit load; the results show a growing difference for curvatures higher than the limit curvature. Kinematic hardening, with the yield surface moving in the direction of the stress increment, yields substantially lower growth of ovalization; as a consequence, the large discrepancy in the predicted value of critical curvature.

The above results reinforce the adequacy of deformation theory for monotonic loading recommended in [11–13]. For cyclic loading, strictly incremental plasticity models are used. The models used are

(a) kinematic hardening (Ziegler),
(b) kinematic hardening (extended Phillips),
(c) the Mroz multisurface model.

(a) and (b), as developed in the previous section, make use of one and two surfaces, respectively. All parameters needed for their implementation can be found in Fig. 8. Parameters for (c) were obtained by approximating the monotonic and stable loops by ten linear segments. Distinction was made between the monotonic and stable loops for better accuracy. The monotonic curve approximation was used strictly for initial loading. The stable hysteresis loop was used for all subsequent paths. The cyclic hardening

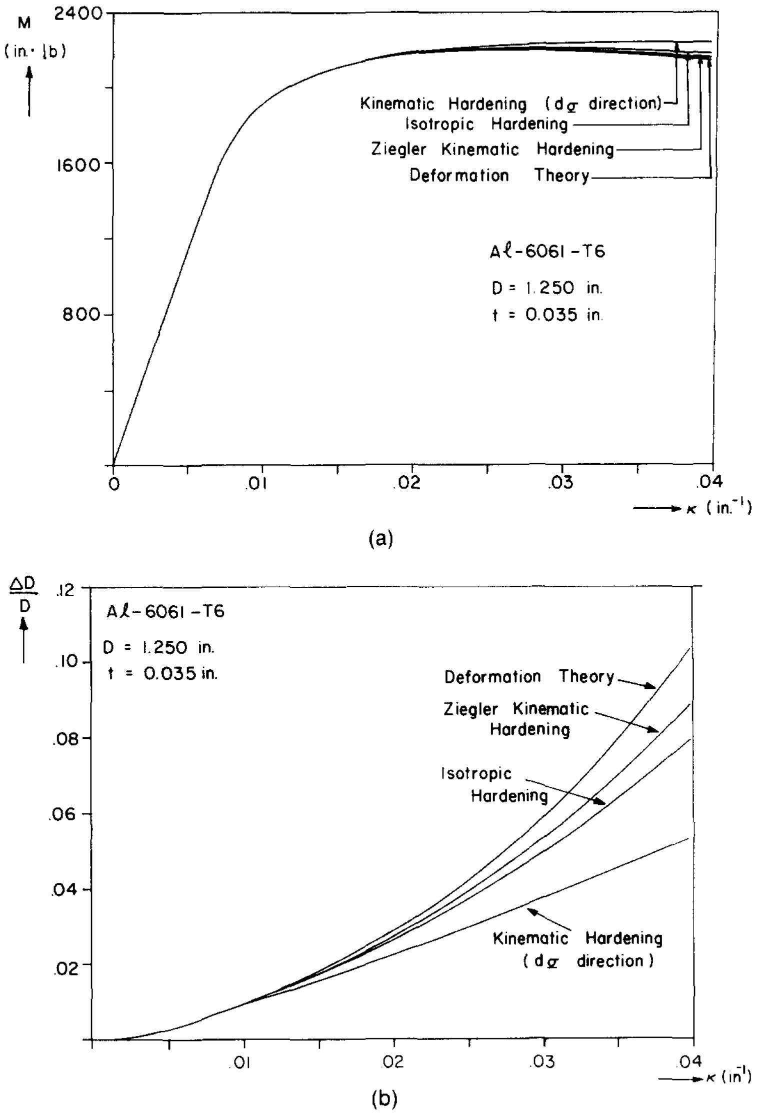

Fig. 9. (a) Monotonic curvature response predicted by various plasticity models. (b) ovalization predicted by various plasticity models for monotonic loading.

observed in the uniaxial tests was introduced in the fashion recommended by Mroz in [18].

The main characteristics of the phenomenon modeled were shown in Fig. 1. Particular emphasis must be given to Figs. 1(b) and 1(c) where the change of the tube diameter (minor diameter) is plotted as a function of curvature and the applied moment, respectively. The progressive growth of ovalization with repeated cycling is clearly visible. Substantial difference is observed between the monotonic and subsequent responses. For loading beyond the monotonic the responses are characterized by a number of symmetries.

For the cases of curvature-symmetric cyclic loading, all three plasticity models mentioned above yielded moment–curvature relationships which represent quite adequately the experimental responses at least for the first few cycles. This should be expected in view of the fact that the induced ovalization is a secondary effect which does not affect very much the moment–curvature response (affects its stability however) for relatively thick ($D/t < 50$) metal tubes. The real test of the model comes from its capacity to predict the cycle-induced ovalization of the cross-section. A measure of the demands of the problem on the plasticity model can be obtained from Fig. 10(a). The stress history of point A (outermost point in plane of symmetry of cross-section) is plotted for 3½ cycles. The highly nonproportional nature of the stress path is clearly seen. For the most part the ratio of the two stresses σ_x/σ_θ is approximately four. The presented results were obtained by using kinematic hardening with the extended Phillips hardening rule. The equivalent stress–strain path followed by the same point is plotted in Fig. 10(b). In view of the curvature-symmetric load history induced to the structure, this path is close to being strain symmetric. The effect of cyclic hardening on this response is observed to be small for this particular material.

Unfortunately, the success indicated for the prediction of moment–curvature response for all models is not repeated in the prediction of the ovalization growth. This is demonstrated in Fig. 11. For convenience the cycle is marked with four points representing the extreme values of the applied curvature. Points (1) and (3) are plotted for a case where the tube examined was cycled to curvature κ_c = 0.020 in.$^{-1}$ (.779 × 10^{-3} mm^{-1}). The predictions of the three models are compared with the experiment. The analysis does not predict any difference between (1) and (3). The extended Phillips model, with an empirically chosen value of β = 0.333 (see Fig. 8), is seen to yield ovalization growth which compares well with experiment. The kinematic hardening rule with Ziegler hardening direction yields an unacceptably high growth of ovalization. The Mroz model yields results closer to the measured, but the rate of growth of ovalization is still a factor of two off. The same trend was shown for higher as well as lower

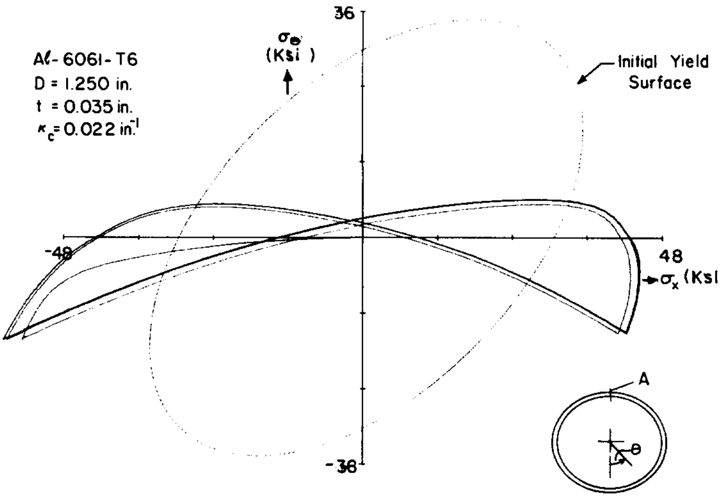

Fig. 10. (a) Predicted stress history at A.

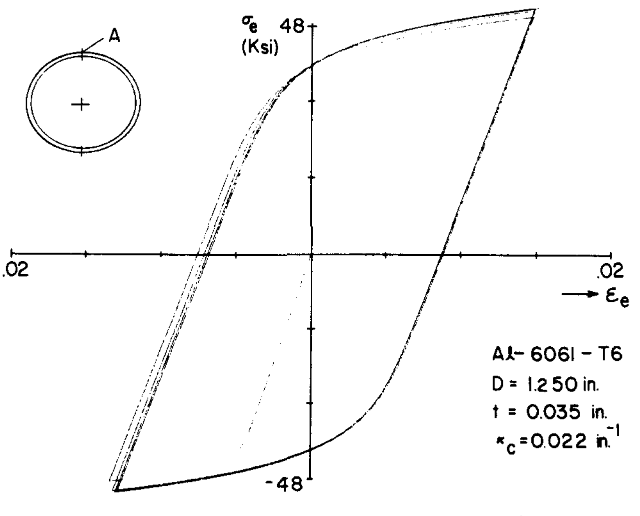

Fig. 10. (b) Equivalent stress–strain history at point A.

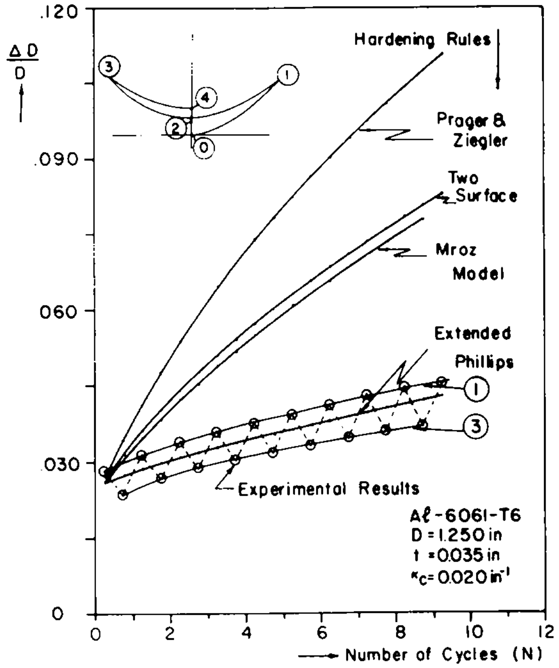

Fig. 11. Cyclic growth of ovalization predicted by various hardening rules.

values of cycling curvature κ_c. Results obtained from using the two-surface model, described earlier, but with the yield surface translating strictly as a Mroz[18] surface [see eqn (26)] are also presented. It is observed that the predictions of this model and those from a ten-surface Mroz model do not differ very much. It would be of interest to test the validity of this near equivalence in other problems also.

Lamba and Sidebottom[37, 38] compared the response predicted by kinematic hardening and the Mroz model in a rather demanding tension–torsion test. Cyclic effects were avoided by first cyclically stabilizing the material. The kinematic hardening rule with Prager- or Ziegler-type hardening direction were found to yield unacceptable results in a strain history involving repeated loading and unloading. The Mroz model was found to yield adequately good comparison. The inadequacy of the Prager or Ziegler hardening direction is also observed in the present problem. The Mroz model performs better but not to an acceptable level. The difference in the performance level of the Mroz model in the two problems is probably related to the different demands applied by the different stress path of most points in the tube and that induced by the tension–torsion experiment of Lambda and Sidebottom.

Figure 12 shows a comparison between experimental and theoretical predictions of moment–curvature. The comparison is quite good. Similar success was obtained for tubes cycled at different curvatures. Figures 13 and 14 show a similar comparison of the ovalization as a function of curvature for two different values of cycling curvature. The kinematic hardening rule with the extended Phillips hardening direction was used. Small differences between the theoretical and predicted results can be observed. The monotonic loading response of the first quarter cycle is particularly different. Although better accuracy in this part of the response could be achieved by adjusting the material parameters, its accuracy was sacrificed in the interest of higher accuracy in the remainder of the response.

In general the predicted results compare well with the experimental ones, in spite of the rather simple plasticity model used. In addition to the limitations of the plasticity model the following factors may have attributed to the observed differences between theory and experiment. The tubes used have initial geometric imperfections in the form of initial ovality, initial eccentricity and other less well-defined thickness variations

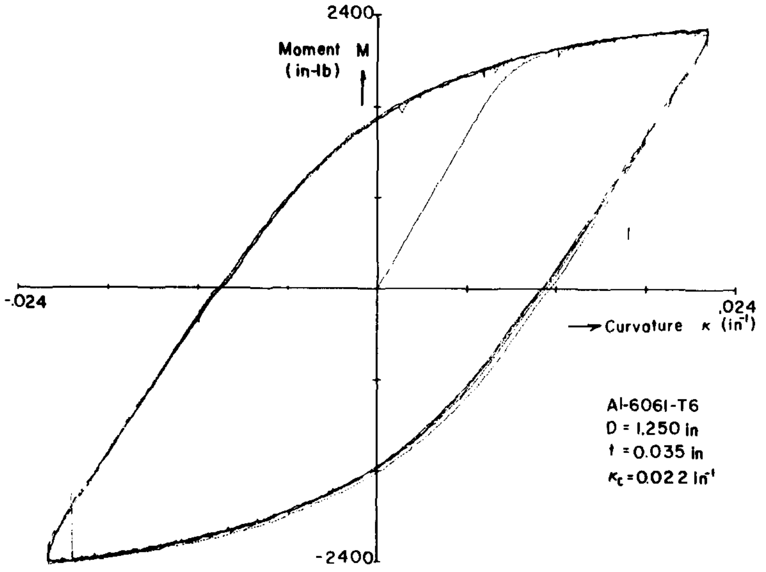

(a) Experiment

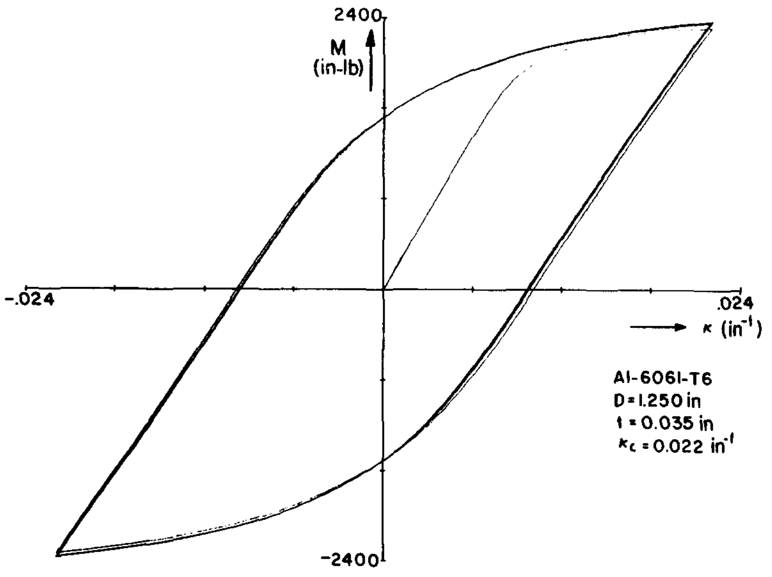

(b) Theory

Fig. 12. Comparison of experimental and theoretical moment–curvature response, $\kappa_c = 0.022$ in.$^{-1}$.

introduced in the drawing process used for manufacturing such tubes. Such imperfections vary along the length of the tube. Although the effect of initial uniform ovality was considered and found to be small, no longitudinally varying imperfections were considered in view of the limitations of the present formulation. For cycling curvatures close to the limit curvature, longitudinal ripples have been repeatedly observed on the compression side of the tube. The relation of any of these ripples to the initial imperfections has not been established. It must be noted that such ovalization nonuniformities were relatively small for curvatures less than about 85–90% of the limit curvature. In view of this, the assumptions of the theory used are judged to be quite adequate for

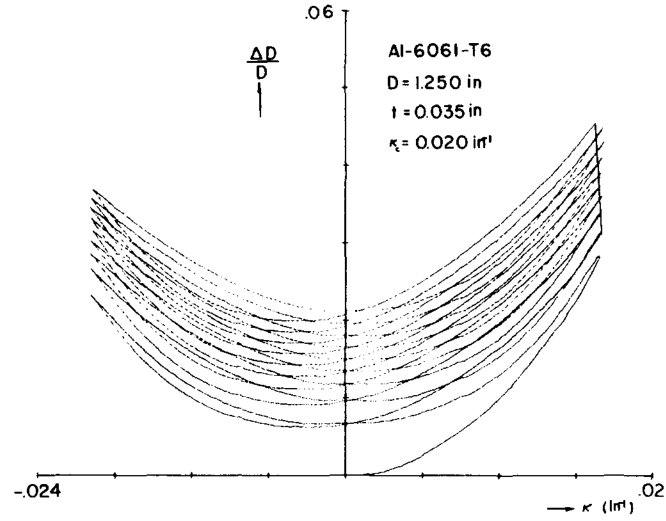

(a) Experiment

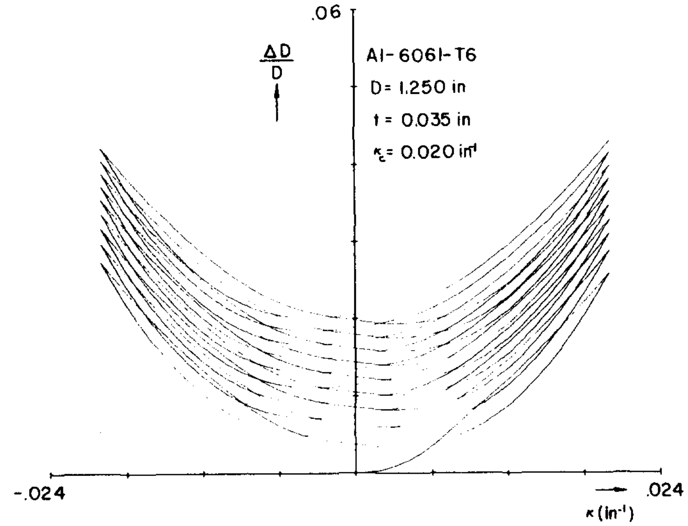

(b) Theory

Fig. 13. Comparison of experimental and theoretical ovalization–curvature response, $\kappa_c = 0.022$ in.$^{-1}$.

the cases presented. Additional sources of error can be attributed to initial material anisotropies and residual stresses that might be present in the tubes used. The effect of residual stresses is not known. The effect of one type of material anisotropy is examined below.

It is also noted that aluminum 6061-T6 exhibits some viscoplastic characteristics at room temperature. Load relaxation was, for instance, observed in the bending experiments in particular at high strain levels. All time-dependent phenomena have been neglected in the present formulation. In view of the loading rate and rather short time span of the experiment, it is felt that this simplification does not unduly bias the results.

The presented results suggest that at least for the particular problem examined in this paper, the Palgen–Drucker model is quite adequate provided a proper kinematic relation governing the movement of a suitably chosen yield surface in stress space is used. It must however be emphasized that this conclusion has been drawn from application of the theory to strictly curvature-symmetric cycles of the tube. This loading path leads to nearly strain-symmetric paths [see Fig. 10(b)] for most points on the tube cross-section. More demanding loading paths which lead to more irregular stress or strain paths will have to be applied to test the model in a more complete fashion.

The extended Phillips hardening rule also requires further study and development in spite of its encouraging performance in the problem examined. In particular, no rational way for establishing the function $h(\xi)$ in eqn (18) is currently available. The authors used a simple form of $h(\xi)$, i.e. eqn (20). The implications of this were explained in the previous section. The validity of this assumption must be questioned and tested in careful biaxial experiments. The efffect of the value of β chosen on the growth of ovalization, is shown in Fig. 15. If β is chosen to be very large, the yield surface translates mainly according to the Mroz hardening rule [expression (26)] applied to the two-surface model. In this case the rate of growth of ovalization is very close to the one predicted by the multisurface Mroz model. On the other extreme, if the yield surface is allowed to translate almost exclusively in the $d\sigma$ direction (e.g. $\beta = 0.067$), then

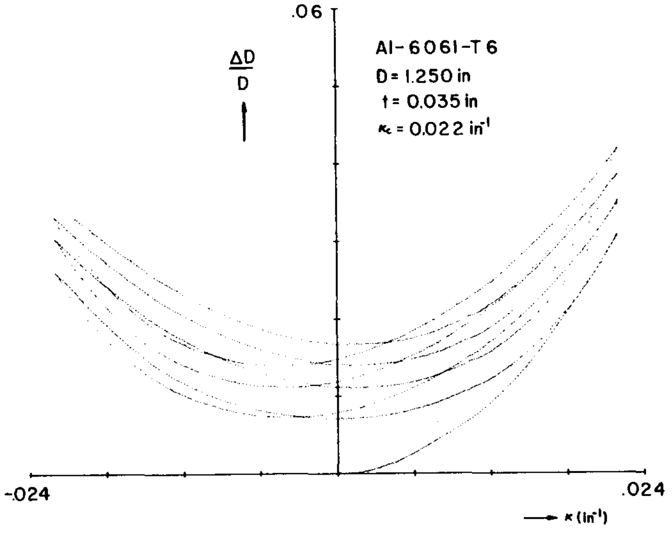

(a) Experiment

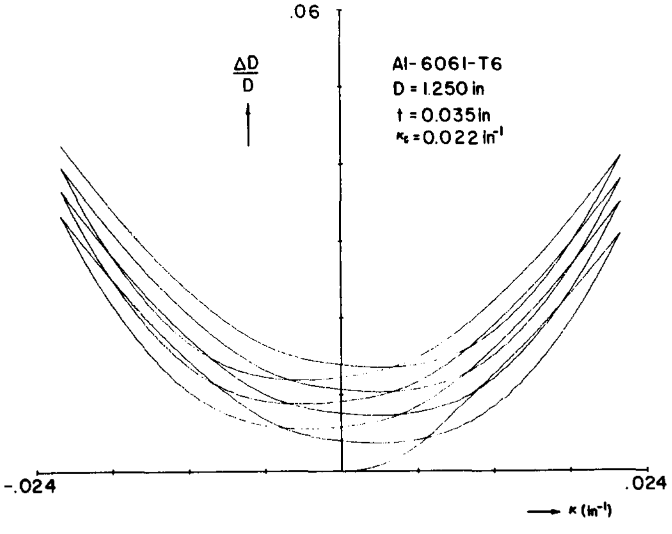

(b) Theory

Fig. 14. Comparison of experimental and theoretical ovalization–curvature response, $\kappa_c = 0.020$ in.$^{-1}$.

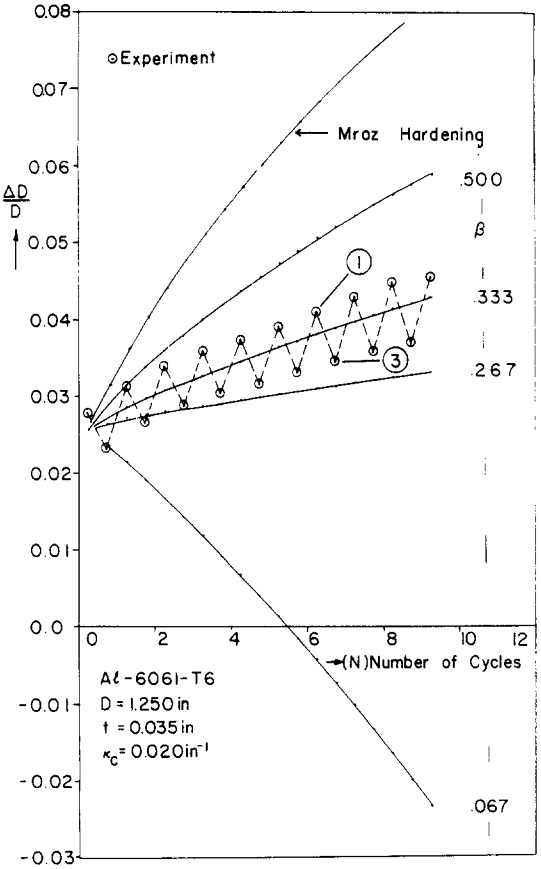

Fig. 15. Effect of parameter β on cyclic growth of ovalization.

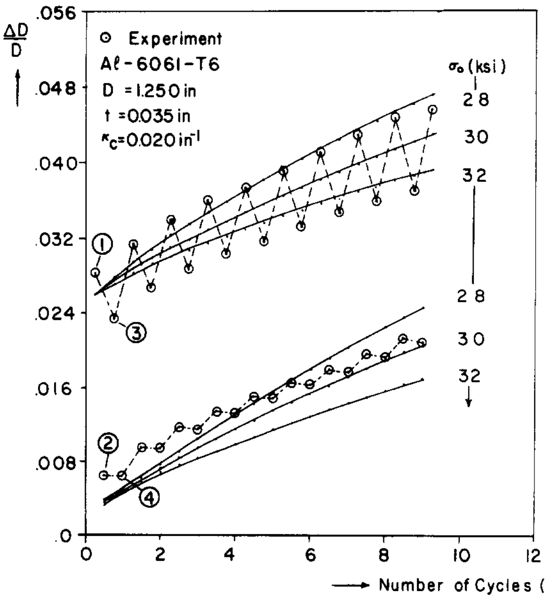

Fig. 16. Effect of choice of yield-surface size on cyclic growth of ovalization.

a negative growth of ovalization is predicted which is physically unacceptable. It is noted that if the $d\sigma$ direction is used exclusively, then the solution procedure fails (diverges) after one or two load reversals. As the value of β is varied, the ovalization growth varies as shown in the figure. The value of $\beta = 0.333$, used in the presented results, was obtained empirically by comparing the experimental and predicted results. It is hoped that the presented results will stimulate discussion and further work on the subject. It would be of great interest, for instance, to know if a function like $h(\xi)$ could be established from strictly uniaxial tests.

As pointed out in [16], the choice of yield-surface size is of prime importance and can affect the results. The effect of choice of yield-surface size on the ovalization growth is shown in Fig. 16. Future users of this model are encouraged to carry out similar parametric studies. It must be clear to the reader that the comparative study of the various plasticity models carried out is far from exhaustive; as a result, any conclusions drawn should be viewed as applying strictly to the particular problem studied and within the confines of the assumptions made.

The reader is reminded that the model used assumes the yield surface to retain its size and shape. In addition, the surface was assumed to be of the Mises type. Under these conditions the direction of translation of the surface in stress space was shown to be of paramount importance to the accurate prediction of the growth of ovalization. It is not clear at this stage whether the same conclusion would be true in the case of more complicated models allowing for surface changes in shape and size.

The effect of one particular type of material anisotropy on the ovalization growth is shown in Fig. 17. It is assumed that the yield stresses in the x and θ directions are different. The Hill anisotropic yield criterion[39] reduced to the two-principal stress state pertinent to this problem can be written as

$$\sigma_x^2 - \sigma_x\sigma_\theta + \left(\frac{1+\lambda}{2}\right)\sigma_\theta^2 = \sigma_0^2, \tag{40}$$

where λ is a measure of the anisotropy. For an isotropic material $\lambda = 1$. Equation (40) is assumed to represent the initial yield surface. Suitably modified for kinematic hardening, (40) replaces (7) in the two-surface model. It was used in conjunction with the extended Phillips hardening direction to solve the cyclic problem at hand. The results shown in Fig. 17 indicate that material anisotropy can affect the growth of ovalization

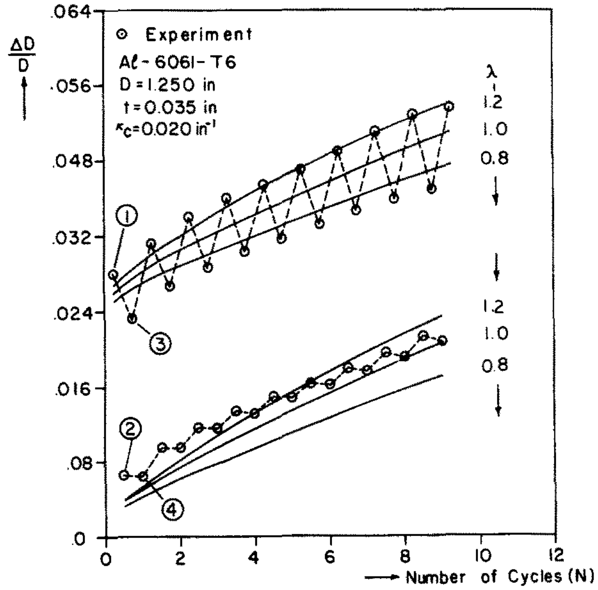

Fig. 17. Effect of material anisotropy on cyclic growth of ovalization.

to the extent shown. Preliminary measurements carried out on the tubes used, indicate that the anisotropy did not exceed the value of λ = 1.4.

Acknowledgements—The reported work was supported in part by the National Science Foundation through Grant CEE-8305951. This support is gratefully acknowledged. The partial support of the first author by the University of Texas during the period of his studies is also acknowledged. We are also indebted to Dr. C. G. Langner for pointing out[40] an application of the problem in offshore structures. The patience shown by Ms. Mary Lou Aiken in typing the manuscript was greatly appreciated.

REFERENCES

1. H. Krawinkler and M. Zohrei, Cumulative damage in steel structures subjected to earthquake ground motions. *Comput. Struct.* **16,** 531–541 (1983).
2. S. Toma and W. F. Chen, Inelastic cyclic analysis of pin-ended tubes. *ASCE J. Struct. Div. ST10.* **108,** 2279–2794 (Oct. 1982).
3. S. Toma and W. F. Chen, Cyclic inelastic analysis of tubular column sections. *Comput. Struct.* **16,** 707–716 (1983).
4. L. F. Kahn and R. D. Hanson, Inelastic cycles of axially loaded steel members. *ASCE J. Struct. Div. ST5.* **108,** 947–959 (May 1976).
5. A. B. Higginbotham and R. D. Hanson, Axial hysteretic behavior of steel members. *ASCE J. Struct. Div. ST7* **102,** 1365–1381 (July 1976).
6. E. P. Popov, V. A. Zayas and S. A. Mahin, Cyclic inelastic buckling of thin tubular columns. *ASCE J. Struct. Div.* **105,** 2261–2277 (1979).
7. V. A. Zayas, S. A. Mahin and E. P. Popov, Ultimate strength of steel offshore structures. *Proc. 3rd Int. Conf. on Behavior of Offshore Structures.* Vol. 1, pp. 39–58. MIT, Boston, Massachusetts (Aug. 1982).
8. L. G. Brazier, On the flexure of thin cylindrical shells and other "thin" sections. *Proc. Roy. Soc. Ser. A.* **116,** 104–114 (1927).
9. E. Reissner, On finite pure bending of cylindrical tubes. *Oesterr. Ing. Arch.* **15,** 165–172 (1961).
10. E. Reissner and H. J. Weinitschke, Finite pure bending of cylindrical tubes. *Q. Appl. Math.* **20,** 305–319 (1963).
11. C. S. Ades, Bending strength of tubing in the plastic range. *J. Aerosol. Sci.* **24,** 605–610 (1957).
12. S. Gellin, The plastic buckling of long cylindrical shells under pure bending. *Int. J. Solids Struct.* **16,** 397–407 (1980).
13. S. Kyriakides and P. K. Shaw, Response and stability of elastoplastic circular pipes under combined bending and external pressure. *Int. J. Solids Struct.* **18,** 957–973 (1982).
14. S. Kyriakides and P. K. Shaw, Buckling of plastic tubes under cyclic bending. *Proc. 4th Eng. Mech. Div., ASCE Spec. Conf.* Vol. I, pp. 604–667. Purdue University (1983).
15. S. Kyriakides and P. K. Shaw, *Inelastic Buckling of Tubes Under Cyclic Bending.* University of Texas Publications, EMRL Report No. 85/4 (1985).
16. D. C. Drucker and L. Palgen, On stress–strain relations suitable for cyclic and other loading. *ASME J. Appl. Mech.* **48,** 479–485 (Sept. 1981).
17. W. D. Iwan, On a class of models for the yielding behavior of continuous and composite systems. *ASME J. Appl. Mech.* **34,** 612–617 (Sept. 1967).
18. Z. Mroz, On the description of anisotropic workhardening. *J. Mech. Phys. Solids* **15,** 163–175 (1967).
19. Z. Mroz, An attempt to describe the behavior of metals under cyclic loads using a more general workhardening model. *Acta Mech.* **7,** 199–212 (1969).
20. Z. Mroz and N. C. Lind, Simplified theories of cyclic plasticity. *Acta Mech.* **22,** 131–152 (1975).
21. W. Prager, The theory of plasticity: a survey of recent achievements. *Proc. Inst. Mech. Eng. London* **169**(21), 41–57 (1955).
22. W. Prager, A new method of analyzing stresses and strains in work-hardening plastic solids. *ASME J. Appl. Mech.* **23,** 493–496 (1956).
23. R. T. Shield and H. Ziegler, On Prager's hardening rule. *ZAMP* **9a,** 260–276 (1958).
24. H. Ziegler, A modification of Prager's hardening rule. *Q. Appl. Math.* **17,** 55–65 (1959).
25. A. Phillips and C. W. Lee, Yield surfaces and loading surfaces: Experiments and Recommendations. *Int. J. Solids Struct.* **15,** 715–729 (1979).
26. A. Phillips, J. L. Tang and M. Ricciuti, Some new observations on yield surfaces. *Acta Mech.* **20,** 23–39 (1974).
27. M. J. Michno and W. N. Findley, Subsequent yield surfaces for annealed mild steel under servo-controlled strain and load histories: Aging, normality, convexity, corners Bauschinger and cross effects. *ASME J. Eng. Mater. Tech.* **97,** 25–32 (1975).
28. J. Morrow and G. M. Sinclair, Cycle-dependent stress relaxation. Symposium on Basic Mechanisms of Fatigue, *ASTM STP* **237,** 83–109 (1958).
29. J. Morrow, Cycle plastic strain energy and fatigue of metals. *ASTM STP* **378,** 45–84 (1965).
30. E. Krempl, Cyclic plasticity: Some properties of the hysteresis curve of structural metals at room temperature. *ASME J. Basic Eng.* **93D,** 317–323 (June 1971).
31. H. R. Jhansale, A new parameter for the hysteretic stress-strain behavior of metals. *ASME J. Eng. Mater. Tech.* **97,** 33–38 (Jan. 1975).
32. M. A. Eisenberg, A generalization of plastic flow theory with application to cyclic hardening and softening phenomena. *ASME J. Eng. Mater. Tech.* **98,** 221–228 (July 1976).
33. D. A. Caulk and P. M. Naghdi, On the hardening response in small deformation of metals. *ASME J. Appl. Mech.* **45,** 755–764 (Dec. 1978).

34. ABAQUS Computer Code. Hibbit, Karlsson & Sorenson Inc., Providence, Rhode Island (1975).
35. O. Fabian, Collapse of cylindrical elastic tubes under combined bending, pressure and axial loads. *Int. J. Solids Struct.* **13,** 1257–1270 (1977).
36. O. Fabian, Elastic–plastic collapse of long tubes under combined bending and pressure load. *Ocean Eng.* **8,** 295–330 (1981).
37. H. S. Lamba and O. M. Sidebottom, Cyclic plasticity for nonproportional paths: Part 1—Cyclic hardening, erasure of memory and subsequent strain hardening experiments. *ASME J. Eng. Mater. Tech.* **100,** 96–103 (Jan. 1978).
38. H. S. Lamba and O. M. Sidebottom, Cyclic plasticity for nonproportional paths: Part 2—Comparison with predictions of three incremental plasticity models. *ASME J. Eng. Mater. Tech.* **100,** 104–111 (Jan. 1978).
39. R. Hill, *The Mathematical Theory of Plasticity*. p. 318. Oxford University Press, London (1950).
40. C. G. Langner, Cyclic bend tests. private communication.

APPENDIX

In the problem of symmetric cyclic bending of tubes, points on the tube cross-section experience cyclic loading to different strain ranges depending on their distance from the neutral axis. It is thus important that the plasticity model used has the capacity of simulating one-dimensional cyclic material behavior well in all strain ranges. In what follows, a small modification to [16] is suggested with the purpose of ensuring that strain-symmetric uniaxial cycling leads to a stable loop which has its maximum stress points on the cyclic stress–strain curve for all strain ranges. Jhansale[31] observed that stable hysteresis loops from experiments at different strain levels are part of the same fundamental shape after suitable translation. In view of this, we make use of the hysteresis loop obtained from a uniaxial experiment of some bounding value of strain. This curve suitably fitted is incorporated in (12) instead of a fit of its lower or upper branch as recommended in [16]. For smaller ranges of strain this curve will be translated in the stress–strain plane by defining a "yield range increment" like parameter[31] y (Fig. A.1). Thus (12) is written as

$$d\epsilon_{ij}^{p} = \frac{1}{\frac{28}{27}\frac{E_s}{n_s}\sigma_0^2}\left(\frac{\sigma_e + y}{\sigma_{ys}}\right)^{n_s-1}[(s_{mn} - a_{mn})\,ds_{mn}]\,(s_{ij} - a_{ij}). \tag{A.1}$$

For cyclically stable material, UVW in Fig. A.1 must coincide with the cyclic stress–strain curve AOA' at $\epsilon = \epsilon_t$. Let σ_t be the stress corresponding to ϵ_t on AOA', i.e.

$$\epsilon_t = \frac{\sigma_t}{E_c}\left[1 + \frac{3}{7}\left(\frac{\sigma_t}{\sigma_{yc}}\right)^{n_c-1}\right], \tag{A.2}$$

then

$$\left(\frac{y + \sigma_t}{E_s}\right)\left[1 + \frac{3}{7}\left(\frac{y + \sigma_t}{\sigma_{ys}}\right)^{n_s-1}\right] = 2\epsilon_t + \left(\frac{y - \sigma_t}{E_s}\right) \tag{A.3}$$

and

$$y = \left[\frac{14}{3}\sigma_{ys}^{n_s-1}(\epsilon_t E_s - \sigma_t)\right]^{1/n_s} - \sigma_t. \tag{A.4}$$

Cyclic hardening can be modeled by modifying (A.4) to include a cycle-dependent hardening parameter as

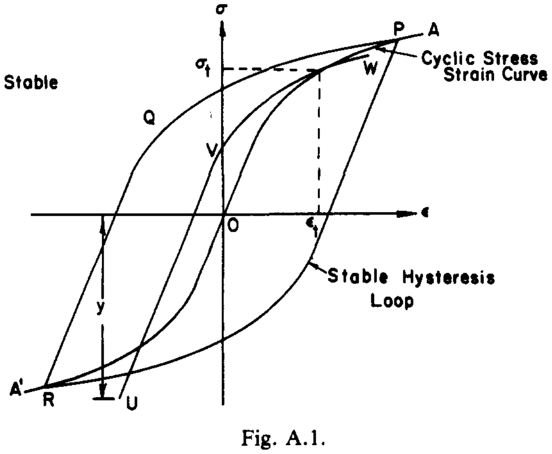

Fig. A.1.

follows:

$$y = \left[\frac{14}{3}\sigma_{ys}^{n_s - 1}(\epsilon_t E_s - \sigma_t)\right]^{1/n_s} - \sigma_t + A(\sigma_t - \sigma_e^{\max}). \qquad \text{(A.5)}$$

A is a material constant governing cyclic hardening and is found from experiments; $\sigma_e^{\max}$ represents the maximum value of equivalent stress reached in the cyclic process.

This formulation has been shown to adequately model cyclic hardening, softening and relaxation. Cyclic creep and paths involving repeated cycling at a mean stress level other than zero require more careful modeling.